Hindawi
Geofluids
Volume 2022, Article ID 2794446, 13 pages
https://doi.org/10.1155/2022/2794446

Research Article

Relationship between Permeability Coefficient and Fractal Dimension of Pore in Ionic Rare Earth Magnesium Salt Leaching Ore

Dan Wang[1], **Yunzhang Rao**[1], **Liang Shi**[1,2], **Wei Xu**[3] and **Tao Huang**[1]

[1]*School of Resources and Environmental Engineering, Jiangxi University of Science and Technology, Ganzhou 341000, China*
[2]*School of Resources and Architectural Engineering, Gannan University of Science and Technology, Ganzhou 341000, China*
[3]*The Seventh Geological Brigade of Jiangxi Bureau of Geology, Ganzhou 341000, China*

Correspondence should be addressed to Yunzhang Rao; raoyunzhang@jxust.edu.cn

Received 26 January 2022; Revised 27 May 2022; Accepted 2 July 2022; Published 16 July 2022

Academic Editor: Mingwei Chen

The change of permeability coefficient of ionic rare earth ore is one of the most important factors causing the uncontrollable flow of leaching solution, and the variation of pore structure of the ore body has a great influence on the permeability coefficient. The research on the evolution of the relationship between pore structure and permeability coefficient of ionic rare earths is of great significance for controlling water and soil pollution and improving the leaching rate of rare earths. In this paper, the column leaching test of ionic rare earth was carried out to study the evolution of the relationship between pore structure and permeability coefficient. In the process of $MgSO_4$ solution and deionized water leaching, the T_2 spectrum and inversion image at each time were obtained by nuclear magnetic resonance (NMR). Based on the fractal theory, the pore structure change of the inversion image was quantitatively analysed, and the permeability coefficient of samples at each time of different leaching agents was calculated by using supercritical Dubinin-Redushckevich (SDR) model to analyse the nuclear magnetic resonance T_2 spectrum. The results show that in $MgSO_4$ solution, the permeability coefficient of the sample changes significantly, and the growth rate of pore fractal dimension remains large. By discussing the evolution law of pore fractal dimension and seepage characteristics of ionic rare earth, the mathematical relationship between permeability coefficient and pore fractal dimension of mineral soil samples at different depths is fitted by polynomial function.

1. Introduction

Ionic rare earth ore in southern China mainly occurs in clay minerals of the weathered granite layer in the form of hydrated cations or hydroxyl hydrated cations [1], and the content of medium and heavy rare earth elements is relatively high, so it is of great value. At present, in situ leaching technology is widely applied to extract effectively rare earth ions from soil. Compared with pool leaching, heap leaching, and other mining technologies [2], in situ leaching technology has the advantages of higher efficiency, lower cost, and more environmental friendly. However, in the process of in situ leaching, a large amount of leaching solution is injected into the ore body through the injection wells and the pore distribution in the ore body changes in real time, leading to the change of ore body permeability [3]. The result shows that the shape of pore channels and the state of their communication paths control the permeability of ore body. With the increase of porosity in ore body, the more channels and the better connectivity, the better the permeability of ore soil, which is beneficial to the infiltration and diffusion of leaching solution in the ore soil layer. Then, the larger the surface area of the leaching reaction, the larger the leaching reaction rate [4]. Hence, it is of great significance to study

Figure 1: Sampling site of ore soil at different depths.

the relationship between ore body pore structure and permeability coefficient in the process of ionic rare earth in situ leaching [5].

According to the interaction between hydrogen protons in the sample and the external magnetic field, the hydrogen proton information is obtained by nuclear magnetic resonance (NMR) technology. NMR is extensively used in porosity measurement and microstructure studies of rock and soil for its three-dimensional, accurate, and nondestructive advantages. Some scholars have explored the relationship between the microstructure of soil particle pores and seepage characteristics by using NMR and electron microscope scanning technology [6]. Under different water content, Dong et al. [7] studied the change rule of soil pore water storage forms based on NMR, and the influence of dry-wet cycle on soil permeability was evaluated. The results showed that in the process of soil wetting, pore water mainly exists in the form of gravity water, and the permeability of soil is proportional to the 6th power of cycle time within 4 cycles. Based on NMR analysis technology, Yang et al. [8] explored the development law of soil permeability of saturated clay in hydrochemical environment and revealed the influence of salt solution concentration on clay permeability by testing the soil pore structure in salt solutions with different concentration. Altunbay et al. [9] studied the relationship between saturation distribution and permeability of rock mass in the longitudinal sections of samples through analysing NMR data. Ausbrooks [10] and other scholars applied the mercury injection method to explore carbonate reservoirs by NMR and found that the pore distribution has a great impact on the permeability coefficient of rock mass. Nakashima and Kikuchi [11] proposed to construct NMR T_2 map to reflect the fracture porosity and permeability coefficient by establishing one-dimensional model. Wu et al. [12] applied NMR to detect the spatial structure and velocity between ore body particles in agar deposits under saturated water condition and obtained velocity field images at three different velocity rates, results showed that the fitting curve diameter of the pore equivalent distribution follows Gaussian distribution, and the velocity distribution in holes is parabolic.

The term fractal was first proposed and used by Mandelbrot. In mathematics, fractal has a strict definition. The so-called fractal refers to the set whose Hausdorff dimension D_h is strictly greater than its topological dimension D_t. Nowadays, the application of fractal has penetrated various disciplines and developed continuously [13]. This is mainly because fractal can express complex objects that cannot be described quantitatively or is difficult to be described quantitatively in a more convenient quantitative method. Relevant studies include the relationship between the fractal dimension of metal fracture and material properties, the relationship between the fractal dimension of rock joint or rock fracture and rock mechanical properties, the relationship between the fractal dimension of pore media and permeability characteristics, etc. In addition, researches also involve the fractal dimension of root form, chemical reaction interface, and soil pores [14]. In practical research, the physical information of the research object can be recorded through various ways, including various graphic image results, for example, photos captured by camera or scanner, micrographs taken by optical microscope or scanning electron microscope, IR images taken by infrared camera, and images obtained by CT technology, AFM technology, and remote sensing technology, even including measurement curves. As these obtained graphics and images contain a lot of physical information of the research object, they are important carriers for us to calculate the fractal dimension. With the development of information processing technology and computer technology, a large number of graphics and images are obtained in the form of digital image, or can be transformed into digital image, which is a two-dimensional matrix represented by a series of binary numbers (0 and 1) after sampling and quantization, has the characteristics of quantization and discretization. Therefore, it has its own characteristics in the calculation of fractal dimension.

Physical fractals in nature often show some randomness and scale, that is, they only show fractal characteristics in a specific scale range from the perspective of statistics [15]. Therefore, there are different ways to define fractal dimension, including Hausdorff dimension D_h, information dimension D_i, similarity dimension D_s, correlation dimension D_g, capacity dimension D_c, spectral dimension D_p, and Lyapunov dimension D_l. For different research objects, different description methods can be used to calculate their fractal dimension.

In general, it is very complicated to determine the Hausdorff dimension D_h of fractals, which restricts its application in practical problems [16]. For fractals with strict self-similarity, it can be proved that the Hausdorff dimension D_h

Table 1: Density of ore samples.

Ore soil depth	Sample number	Volume/cm^3	Mass/g	Natural density/(g/cm^3)	Mean natural density/(g/cm^3)	Mean dry density/(g/cm^3)
3 m	1	50.0	68.51	1.37	1.38	1.26
	2	50.0	67.85	1.36		
	3	50.0	70.38	1.41		
4 m	1	50.0	64.36	1.29	1.29	1.13
	2	50.0	65.47	1.31		
	3	50.0	63.65	1.27		
5 m	1	50.0	78.31	1.56	1.52	1.33
	2	50.0	75.62	1.51		
	3	50.0	74.23	1.48		

Table 2: Particle size percentage content of ore samples at different depths.

Ore soil depth	Particle diameter/mm					
	>5	2.5~5	1~2.5	0.5~1	0.075~0.5	<0.075
3 m	15.8%	32.2%	16.6%	16.2%	10.9%	8.3%
4 m	12.4%	37.3%	18.4%	16.2%	10.8%	4.9%
5 m	10.3%	31.6%	17.6%	18.2%	16.2%	6.1%

is equal to the similarity dimension D_s and the similarity dimension, which is easy to calculate normally, and can be calculated according to the following formula, where N is the number of similarity elements, and r is the similarity ratio of similarity elements.

$$Ds = \frac{\ln N}{\ln (1/r)}. \tag{1}$$

For many fractals, both Hausdorff dimension and similarity dimension are difficult to be calculated, so many equivalent or approximate dimension definitions are proposed. Considering that the image is a surface surrounded by various curves, such as pores and sections, box-counting dimension D_f can be used [17]. Box-counting dimension is a better method to calculate the fractal dimension of two-dimensional image. There are a series of equivalent definitions of boxed dimension, and the approximate calculation method of boxed dimension is the following formula, where N is the number of δ net cubes intersecting F.

$$D_f = \lim_{k \longrightarrow \infty} \frac{\ln N(F)}{\ln \delta}. \tag{2}$$

Currently, a large amount of research on the relationship between pore microstructure and seepage characteristics of soil particles has been done by using NMR and SEM techniques, yet the pore structure analysis and evolution of rare earth ore in leaching process need to be further investigated. Based on the above, the permeability coefficient of mineral soil at different leaching time was calculated by SDR model. In this paper, the pore fractal dimension was introduced using fractal theory, the change of pore structure was described quantitatively, and the evolution of the relationship between pore structure change and seepage characteristics of ionic rare earth mineral soil was discussed.

Table 3: Porosity and pore ratio of ore samples at different depths.

Ore soil depth	3/m	4/m	5/m
Porosity (n)	0.47	0.52	0.45
Pore ratio (e)	1.05	1.25	1.01

Figure 2: Rare earth samples at different depths.

2. Materials and Methods

2.1. Materials. To truly simulate the in situ leaching situation of mines, Luoyang shovel with a diameter of 160 mm was

Figure 3: Low field NMR.

used in this site soil borrowing, after planning the surface humic layer, drilled with Luoyang shovel to 0.5 m for sampling. For every 1 m drilling, we took undisturbed soil samples of fully weathered layers 3 m, 4 m, and 5 m away from the topsoil with a ring knife, took 3 samples at the same depth, a total of 9 samples were taken, and took protective measures to prevent excessive evaporation of water in the subsequent transportation process of soil samples, which would affect the determination of physical properties of undisturbed soil. The excess loose soil of the same depth was packed and brought back in woven bags and marked on the outside of the bags, see Figure 1 for the sampling site of mineral soil.

The mineral soil in this area is generally clayey soil. In this test, the density of samples with different depths was tested by ring knife method. The density measurement results are shown in Table 1. Samples with different depths were screened by sieving method, and the apertures of the sieves were superimposed from large to small, which were 5 mm, 2 mm, 1 mm, 0.5 mm, 0.25 mm, 0.1 mm, and 0.075 mm, respectively, see Tables 2 and 3 for particle size distribution, porosity, and void ratio of samples with different depths.

Based on the difference of physical and chemical properties of undisturbed soils, the soil samples were divided into three groups: A, B, and C according to the height of soil from the surface. Among them, groups A, B, and C represent the ore soil 3 m, 4 m, and 5 m away from the surface, respectively. During the column leaching experiment, to ensure that the sample to be tested was located in the effective detection area of the NMR instrument, mineral soil was added into the acrylic tube in layers and tamped. In addition, each layer of soil sample was treated by surface scratching to prevent the stratification effect of ore soil due to the seepage of leaching solution. A qualitative filter paper and a permeable stone were placed in turn at the bottom of the acrylic tube so that the leaching solution could not only flow out of the system but also prevented the loss of sample microparticles [18]. Finally, the remolded soil sample with diameter-height ratio of 44 mm: 60 mm was obtained, as shown in Figure 2. Furthermore, two samples were set up in each group. One sample was leached with 2% MgSO4 solution (A1, B1, and C1), and the other was leached with deionized water (A2, B2, and C2).

2.2. Experimental Apparatus and Scheme. In this experiment, a MesoMR23-060H-I NMR [19] apparatus was applied. It is mainly composed of magnet, magnet resonance spectrometer, data processing, and image reconstruction (Figure 3). And the relevant parameters are as shown in Table 4. After the sample was put into the instrument for detection, the nuclear magnetic resonance instrument would scan the image of the sample profile, compare it with the preset parameter model, and inversed the image inside the soil column at this time.

To investigate the relationship between permeability coefficient and pore fractal dimension of ion-adsorbed rare earth in $MgSO_4$ solution leaching, column leaching experiments were carried out. The column leaching experiment system consists of a beaker, liquid infusion pipe, and an object stage (Figure 4). The whole leaching procedure is as follows:

(1) After a large number of laboratory experiments and production practices in mining enterprises, the 2% $MgSO_4$ solution was used to leach ore, and the recovery rate can reach 99.7%. In addition, the other ions in the solution could be greatly reduced. Hence, 2% $MgSO_4$ solution was used for column leaching in this experiment. The $MgSO_4$ solution used in the experiment was purchased from local chemical plants

(2) One end of the infusion pipe was inserted into the beaker, and the other end was suspended above the sample. The infusion rate was adjusted to 3 mL/min

Table 4: Technical parameters and test parameters of low field NMR.

Instrument parameters				Test parameters			
Resonant frequency	23.316/MHz	Pulse width P90	18/us	RF delay D3	80/us	Repeated sampling times NS	4
Coil diameter	60/mm	Pulse width P180	36/μs	Sampling duration TR	1000/ms	Scan times	32
Magnet strength	0.52/T	Sampling point TD	266424	Analog gain RG1	20	Echo interval	0.2/ms
Magnet temperature	32/°C	Sampling frequency SW	200/kHz	Numerical gain RG2	3	Echo count	4000

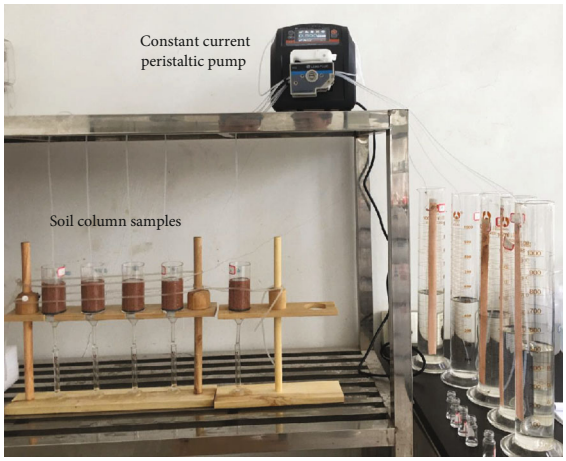

Figure 4: Indoor leaching device.

and turned on the switch of the infusion set. The concentration of RE^{3+} in the leaching solution was analysed by sampling at intervals to judge the leaching process

(3) The samples were put into NMR instrument every one hour for pore structure detection and inversion imaging. Then, the samples were put back into the solution to continue leaching. When the concentration of RE^{3+} in the leaching solution is very low or almost undetectable, it is believed that all rare earth in the samples have been leached and stopped during the column leaching experiment

3. Results and Discussion

3.1. Calculation of Permeability Coefficient. In a pulse environment with a certain frequency, the hydrogen nucleus in the sample absorbs electromagnetic waves with a specific frequency and transitions from low energy state to a high energy state. Then, the magnetization vector deviates from an equilibrium state, the process of the hydrogen nucleus recovering from an unequilibrium state to an equilibrium state is called a relaxation process, and the duration of the process is the relaxation time [20]. Based on the principle, two types of permeability coefficient calculation models are proposed: (1) Coates model, which is suitable for laminar flow of water or hydrocarbons; (2) average T_2 model, which is suitable for water-bearing pore system. According to the

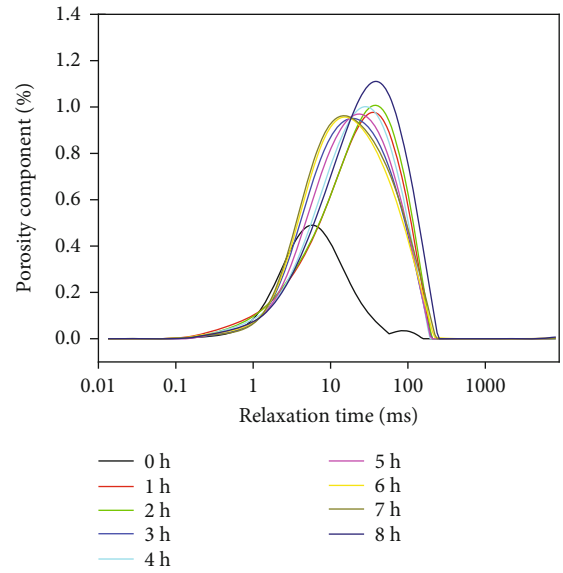

Figure 5: T_2 curves of A1 sample at different leaching times.

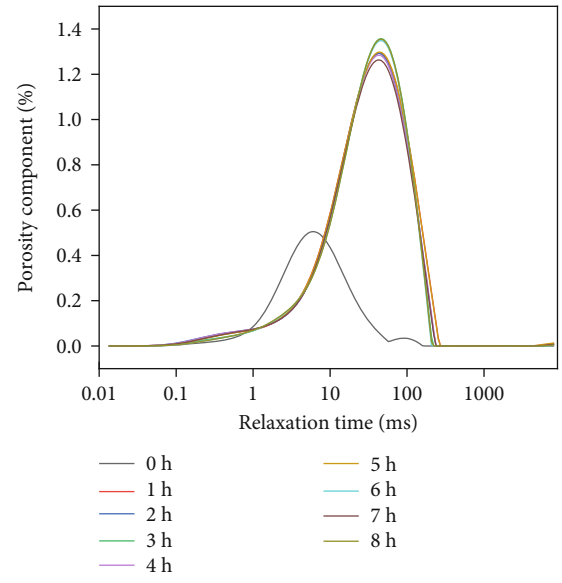

Figure 6: T_2 curves of A2 sample at different leaching times.

relaxation mechanism of NMR, there are three kinds of relaxation in the fluid of pores, namely, free relaxation, surface relaxation, and diffusion relaxation [21]. The transverse

Table 5: Permeability coefficient of samples in each stage of leaching process.

Leaching time/h	Leaching solution	Permeability coefficient K (10^{-5}m/s)			Leaching solution	Permeability coefficient K (10^{-5}m/s)		
		A1	B1	C1		A2	B2	C2
1	Magnesium sulfate solution	1.105	1.425	0.988	Deionized water	0.995	1.258	0.877
2		1.189	1.521	1.025		1.096	1.304	0.893
3		1.347	1.675	1.189		1.154	1.437	1.092
4		1.641	1.984	1.504		1.232	1.492	1.114
5		1.842	2.248	1.649		1.398	1.551	1.158
6		1.856	2.256	1.702		1.406	1.612	1.224
7		1.874	2.267	1.741		1.423	1.618	1.197
8		1.885	2.274	1.759		1.407	1.613	1.166

relaxation time T_2 can be expressed by the following formula:

$$\frac{1}{T_2} = \frac{1}{T_{2B}} + \frac{1}{T_{2\text{surface}}} + \frac{1}{T_{2E}}, \tag{3}$$

where T_{2B} is the free relaxation time of the fluid, ms; since the value of T_{2B} is much greater than T_2, when the magnetic field is uniform and T_{2E} is small enough, formula (3) can be simplified as

$$\frac{1}{T_2} = \frac{1}{T_{2\text{surface}}}. \tag{4}$$

Average T_2 (SDR) model is expressed as

$$K = aT_{2g}{}^{2\varnothing^4}, \tag{5}$$

$$a = F_s \cdot \rho, \tag{6}$$

where $\varnothing$ is the effective porosity of NMR; T_{2g} is the geometric mean of T_2 distribution; a is the parameter related to stratum type; F_s is the pore shape factor and usually takes 3; ρ is the surface relaxation rate of soil samples.

In the leaching process, the samples are in an inorganic hydro chemical environment, and the ions are mainly RE^{3+}, Mg^{2+}, H^+, etc. There are no hydrocarbons in the solution [22]. Therefore, the SDR model can be used to calculate the permeability coefficient of rare earth ore. Xu et al. [23] calculated the surface relaxation rate of rare earth by random walk algorithm, and the surface relaxation rate was 1.36. The obtained data have a good correlation with the permeability measured by indoor simulated leaching. According to the collected T_2 spectrum curves, as shown in Figures 5 and 6, the permeability coefficients of the soil column at each time are calculated and listed in Table 5.

According to the results detected by nuclear magnetic resonance instrument, the porosity of each sample at different times under the action of two leaching fluids over time is summarized. It is shown in Figures 7 and 8 that the fitting curves describe the variation characteristics of permeability coefficient during the leaching process in the two kinds of leaching solutions. In the process of $MgSO_4$ solution leaching, the permeability of samples increases greatly in 6 h. After 6 h, the permeability changes little and tends to stability. In this process, magnesium ions interact with rare earth ions in solution. In 5 h of $MgSO_4$ leaching, the permeability coefficients of A1, B1, and C1 climb gently. 5 h later, the permeability coefficient of each sample has no obvious change. During the deionized water leaching, a small number of microparticles in the ore body migrate, and the permeability coefficient of the sample increases rapidly in 3 h; after 3 h, the microparticles block in the pores in the ore body move to the bottom of the sample with the movement of deionized water, and the permeability coefficient of the sample remains almost unchanged.

3.2. Calculation of Pore Fractal Dimension. With the NMR reconstruction imaging technology, the pore image of ore leaching at each time is inverted and reconstructed [24]. Variation law of the pore microstructure at the leaching moment is analysed by inversion images of the middle longitudinal section of the column [25]. The representative images of 5 stages in the leaching process of group A, Figure 9, are compared with the images of the same stages of deionized water leaching, Figure 10. The whole leaching stage is mainly divided into five stages: water saturation of the sample, initial reaction, effective leaching, residual reaction, and end of reaction.

As shown in Figure 9, the leaching process is completed under the coupling action of seepage field and chemical field. Due to the effect of exchange reaction erosion, the particle shape changes from time to time, and the height of the sample will decrease, with the microparticles in the upper layer migrate downward with the leaching solution and fill the large pore diameter in the lower layer, resulting in the dynamic change of pore micromorphology. The pore radius also changes all the time. In the early stage of leaching, the sample changes from unsaturated state to saturated state, where the liquid buoyancy plays a leading role, and the number of micropores and small holes decreases rapidly. In the effective leaching stage, ion exchange reaction erosion plays a leading role, which changes the particle structure of the sample, decomposes some particles with larger particle size into smaller particles, and increases the proportion of pores below the middle pore, while decreases the proportion of pores above the large pore. As the reaction approaches to

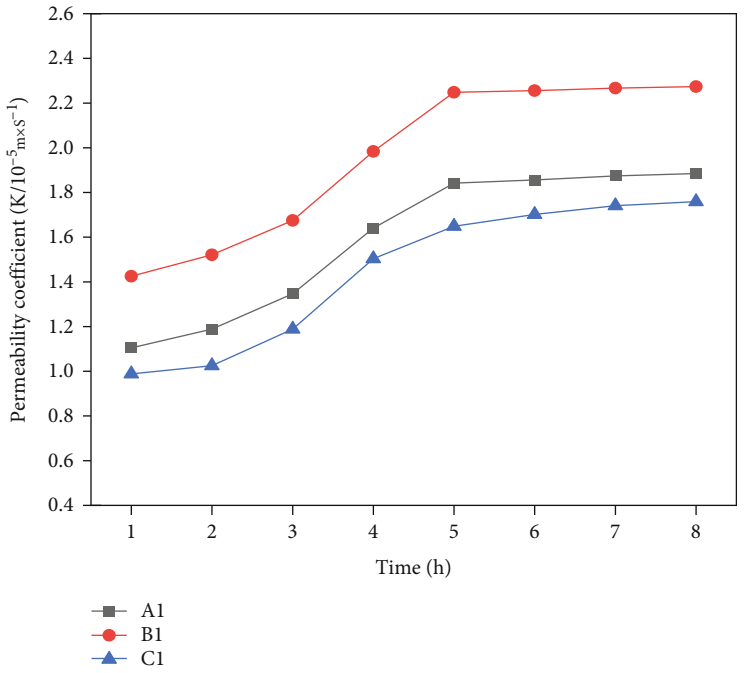

Figure 7: Permeability coefficient of $MgSO_4$ leaching sample.

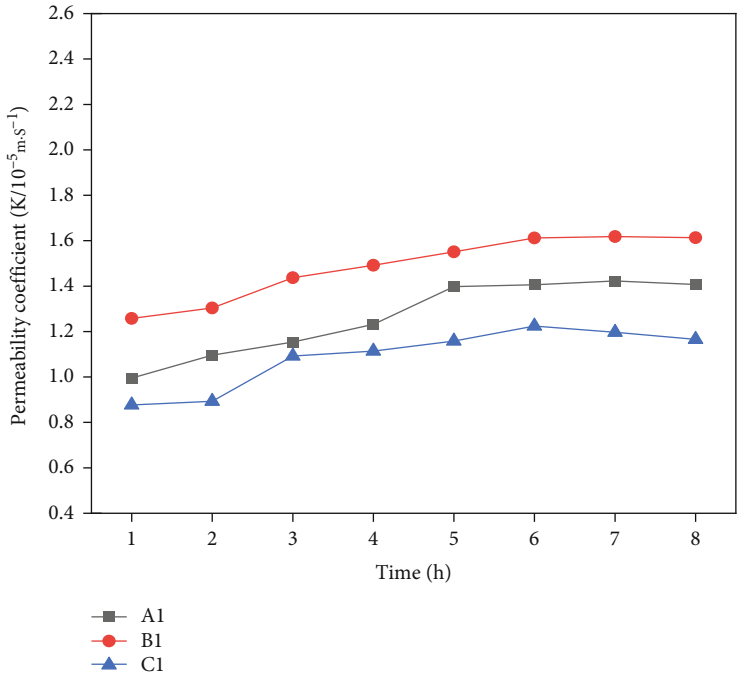

Figure 8: Permeability coefficient of deionized water leaching sample.

the end, the seepage of fluid plays a leading role. Under the action of a certain head pressure, a stable seepage channel is formed in the sample, and the distribution of pore sizes in the sample tends to be stable.

In the process of ion exchange, the positive trivalent rare earth ions are replaced by positive divalent magnesium ions into the solution. According to the principle of charge balance solution, the content of anions in the solution should also increase accordingly, resulting in the dissolution of anions in minerals into the solution, so that the solution can reach the charge balance state again. Due to the anions from the ore particles, the charge balance between the two surfaces is changed. As a result, a large number of uncharged microparticles are deposited on the surface of the ore body

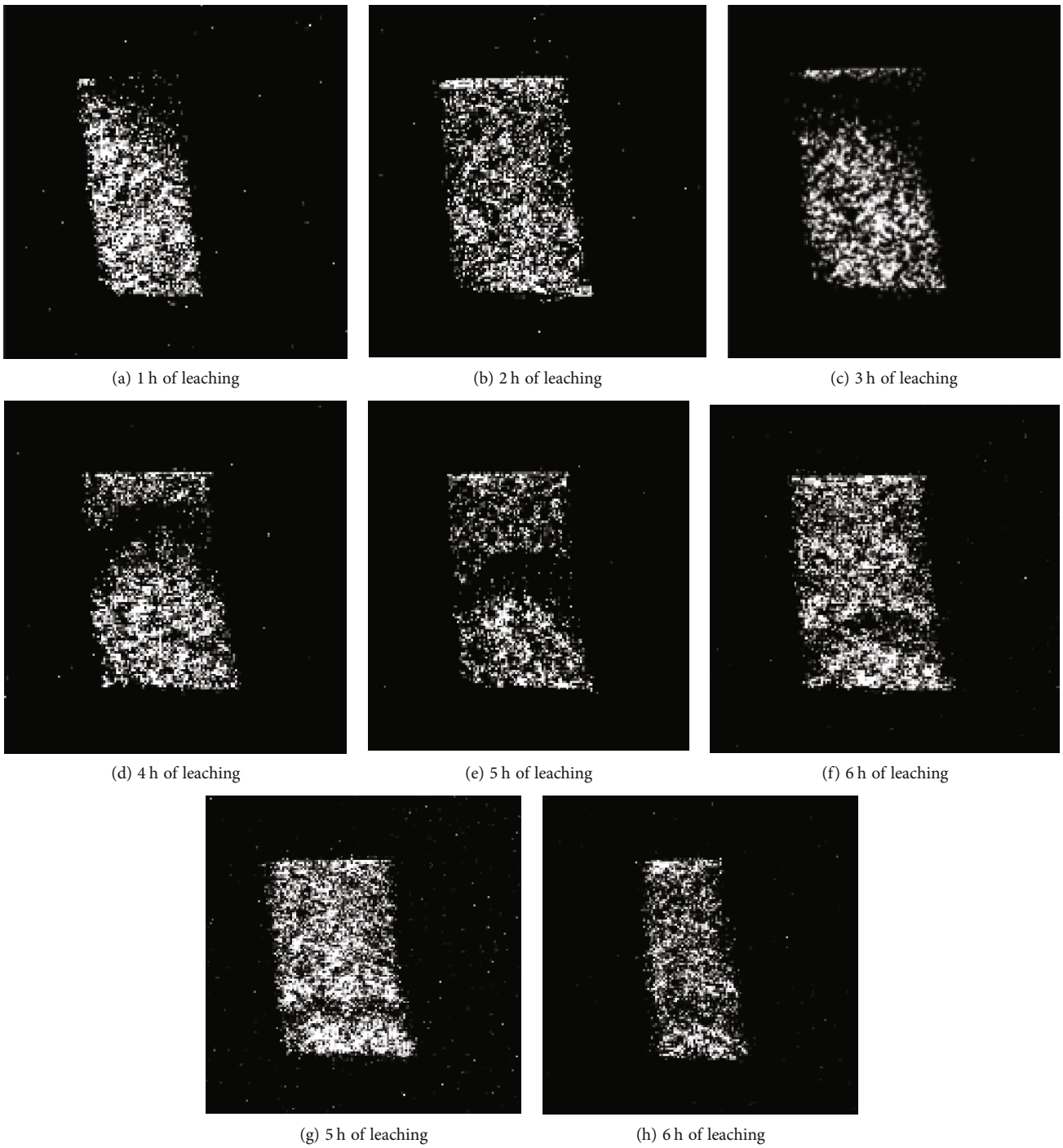

(a) 1 h of leaching (b) 2 h of leaching (c) 3 h of leaching

(d) 4 h of leaching (e) 5 h of leaching (f) 6 h of leaching

(g) 5 h of leaching (h) 6 h of leaching

Figure 9: Vertical axis profile of MgSO4 leaching inversion.

by Coulomb force, filling the pores with large aperture. With the completion of ion exchange reaction, most of the rare earth cations with positive trivalent have been separated from ore, and the thickness of the electric double layer of clay colloidal particles in the colloid will increases again, which will make the repulsion force of the electric double layer become the dominant force again, resulting in the release of the particles adsorbed around the macropores, and the macropores return to their original state, showing a fine pore structure. This shows that the ion exchange process in the leaching process of rare earth ore body will lead to the change of particle morphology and the deposition and release of fine particles in the ore body, resulting in the evolution of dynamic pore structure. At the same time, rare earth ions migrate downward through seepage, resulting in a significant increase in the positive charge content at the bottom of the sample, while the clay containing rare earth usually has a negative charge. Under the action of electric

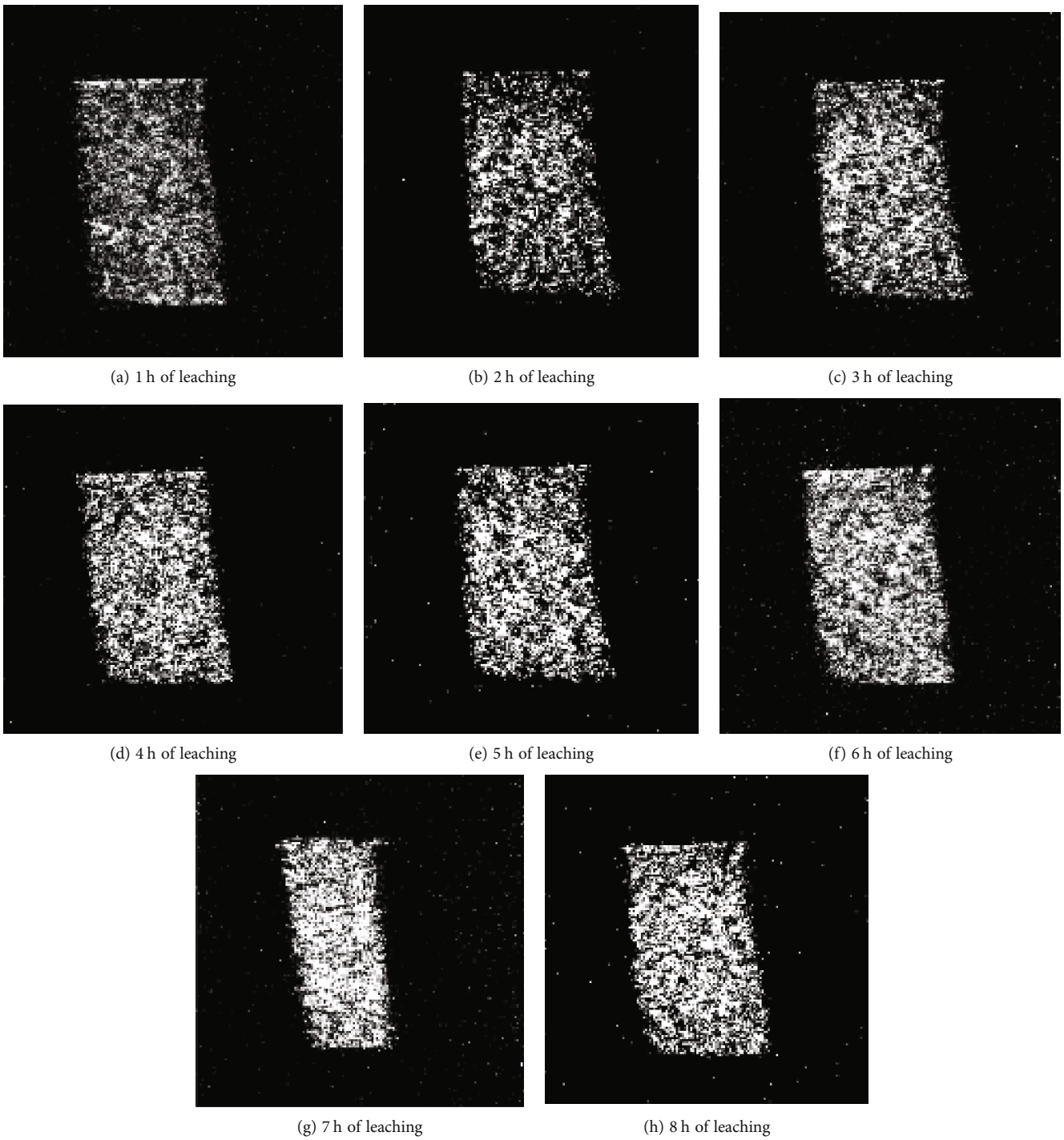

(a) 1 h of leaching (b) 2 h of leaching (c) 3 h of leaching

(d) 4 h of leaching (e) 5 h of leaching (f) 6 h of leaching

(g) 7 h of leaching (h) 8 h of leaching

Figure 10: Vertical axis profile of deionized water leaching inversion.

field force, these clays converge to the bottom of the sample, block the pores at the bottom of the sample, and change the pore structure.

The pore size distribution of soil is described by fractal theory, the microstructure characteristics of particle size can quantitatively describe the pore structure characteristics at each time in the leaching process, and the relationship between pore structure and seepage rule is revealed, to explore the influence of fractal dimension of soil pore on seepage characteristics of soil [26–28].

Pore fractal dimension D_f is a significant parameter to present the microscale change of soil pores [29], which is usually described by the distribution characteristics of pore accumulation number less than the specific pore, as shown in formula (2). In the logarithmic coordinate system, the corresponding relationship between different

Table 6: Fractal dimension of pores in each stage of the sample during ore leaching.

Leaching time/h	Leaching solution	A1		B1		C1		Leaching solution	A2		B2		C2	
		Fractal dimension	Growth rate/%	Fractal dimension	Growth rate/%	Fractal dimension	Growth rate/%		Fractal dimension	Growth rate/%	Fractal dimension	Growth rate/%	Fractal dimension	Growth rate/%
1	Magnesium sulfate solution	1.526	——	1.617	——	1.332	——	Deionized water	1.421	——	1.578	——	1.227	——
2		1.589	4.128	1.742	7.730	1.421	6.682		1.489	4.785	1.624	2.915	1.315	7.172
3		1.678	5.601	1.886	8.266	1.562	9.923		1.524	2.351	1.651	1.663	1.367	3.954
4		1.782	6.198	1.924	2.015	1.689	8.131		1.572	3.150	1.684	1.999	1.414	3.438
5		1.854	4.040	1.943	0.988	1.741	3.079		1.617	2.863	1.702	1.069	1.459	3.182
6		1.924	3.776	1.956	0.669	1.778	2.125		1.648	1.917	1.714	0.705	1.482	1.576
7		1.941	0.884	1.967	0.562	1.794	0.900		1.657	0.546	1.725	0.642	1.491	0.607
8		1.943	0.103	1.971	0.407	1.756	——		1.661	0.241	1.733	0.464	1.502	0.738

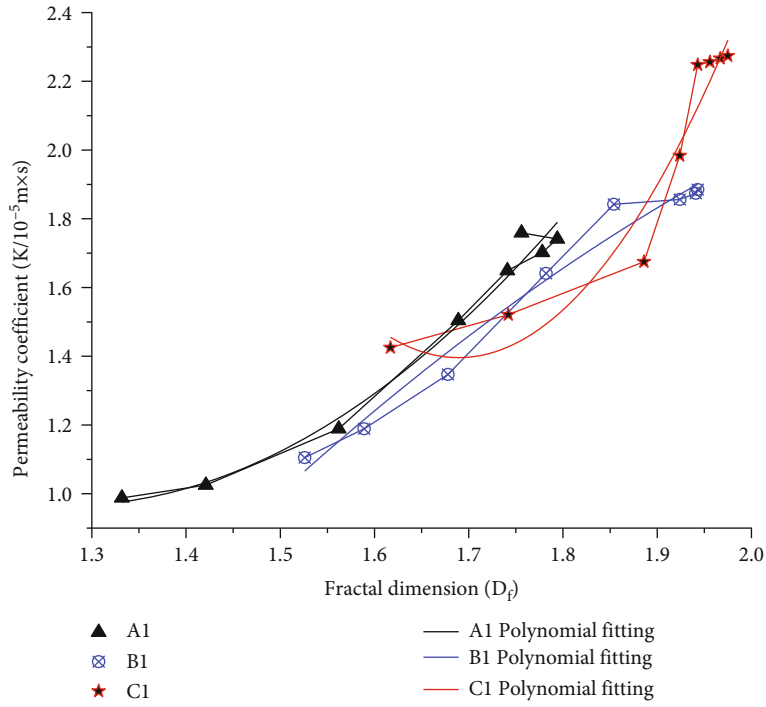

FIGURE 11: Relationship between fractal dimension and permeability coefficient of $MgSO_4$ leaching pores A1: $K = -1.05251 * D_f^2 + 5.65291 * D_f - 5.10929$. B1: $K = 11.31327 * D_f^2 - 38.22234 * D_f + 33.68001$. C1: $K = 3.01795 * D_f^2 - 7.6732 * D_f + 5.84253$.

pore sizes and their corresponding pore numbers was fitted [30].

MATLAB software was used to automatically remove miscellaneous points [31], divided and identified particles and pores, and calculated the fractal dimension of pores in the process of leaching, and the results are given by Table 6. It is clear that the fractal dimension of sample pores increases in the first 6 hours; from this moment onwards, it tends to enter into the comparatively stable period. In $MgSO_4$ solution, the growth rate of fractal dimension keeps at a large value in the effective leaching stage (2 h ~6 h), and the change trend is positively correlated. In deionized water, the fractal dimension increases, while the change trend of fractal dimension growth rate is negatively correlated within 2 h ~6 h. During the leaching process of $MgSO_4$ solution, Mg^{2+} and RE^{3+} in the solution react, which changes the grain structure of ore soil, resulting in the difference of fractal dimension between $MgSO_4$ solution and deionized water.

3.3. Relationship between Pore Structure and Permeability Coefficient. The characteristic parameters of meso structure of soil particles were described by fractal theory, to quantitatively analyse the variation of pore structure during leaching and calculate the permeability coefficient in each leaching stage according to the SDR model [32, 33]. The relationship between the permeability coefficient and fractal dimension was indicated, and the fitting curve was obtained, as shown in Figure 11. In the process of the two solutions of leaching, the permeability coefficient of samples is positively correlated with the fractal dimension of the pores. However, in $MgSO_4$ solution, the internal pore structure changed rapidly resulting from the coupling effect of seepage and ion exchange reaction, leading to the fluid flowing more easily in the pores. The polynomial function is used to fit the relationship between K and D_f. The fitting result shows that in the 95% confidence interval, R^2 is larger than 0.9143.

4. Conclusion

Based on SDR model and classification theory, the permeability coefficient and fractal dimension at different leaching time were calculated. And the evolution of the relationship between pore structure variation and seepage characteristics of ore-soil particles was established. The main conclusions are as follows:

(1) In the leaching process of deionized water, the permeability coefficient rises slightly due to the migration of ore-soil particles, but the growth rate is small; in the leaching process of $MgSO_4$, the permeability coefficient changes significantly, indicating that the change of permeability coefficient is closely related to the internal ion exchange reaction

(2) In the leaching process of deionized water, the fractal dimension increases, while the change trend of fractal dimension growth rate is negatively correlated with time in 2 h ~6 h. In the leaching process of $MgSO_4$, the growth rate of fractal dimension keeps at a large value in the effective leaching stage (2 h ~6 h), and the change trend is positively correlated with time

(3) The relationship between permeability coefficient and fractal dimension shows strong correlation, so

the mathematical relationship between permeability coefficient and fractal dimension can be fitted by polynomial function, and a method for estimating permeability coefficient based on fractal dimension of soil sample is obtained

Data Availability

The data that support the findings of this study are available from the corresponding author (VS) upon reasonable request.

Conflicts of Interest

The authors declare that there are no conflicts of interest regarding the publication of this paper.

Acknowledgments

This research was supported by the National Natural Science Foundation of China (51964014) and the Education Department of Jiangxi Province (GJJ209414).

References

[1] X. W. Zhou, D. X. Wen, and X. P. Luo, "The status quo and development trend of the extraction technology of ion-absorbed rare earth in southern China," *Nonferrous Metals Science and Engineering*, vol. 3, no. 6, pp. 81–85, 2012.

[2] B. Fan, L.-s. Zhao, Z.-y. Feng et al., "Leaching behaviors of calcium and magnesium in ion-adsorption rare earth tailings with magnesium sulfate," *Transactions of Nonferrous Metals Society of China*, vol. 31, no. 1, pp. 288–296, 2021.

[3] H. Zhengyan, Z. Zhang, R.'a. Chi et al., "Leaching hydrodynamics of weathered elution-deposited rare earth ore with ammonium salts solution," *Journal of Rare Earths*, vol. 35, no. 8, pp. 824–830, 2017.

[4] W. Que, Y. Tan, Y. Zeng, and S. Wang, *Geochemical Kinetics and Mass Transport of In Situ Uranium Leaching*, Atomic Energy Press, Beijing, 2004.

[5] S. H. Yin, Y. Qi, F. F. Xie, X. Chen, L. M. Wang, and Y. J. Shao, "Porosity characteristic of leaching weathered crust elution-deposited rare earth before and after leaching," *Chinese Journal of Nonferrous Metals*, vol. 28, no. 10, pp. 2112–2119, 2018.

[6] F. Shang-xin, C. Jun-rui, X. Zeng-guang, Q. Yuan, and C. Xi, "Mesostructural change of soil-rock mixtures based on NMR technology," *Rock and Soil Mechanics*, vol. 39, no. 8, pp. 2886–2894, 2018.

[7] J. G. Dong, H. B. Lv, and G. Q. Chen, "Pore-water form determined by using NMR method and its influence on soil permeability," *Transactions of the Chinese Society of Agricultural Engineering*, vol. 36, no. 6, pp. 74–80, 2020.

[8] D. H. Yang, C. F. Wei, R. T. Yan, Q. Tang, and L. Liu, "Experimental study on effects of fine particle migration and fabric change on permeability of clay," *Chinese Journal of Geotechnical Engineering*, vol. 41, no. 11, pp. 2009–2017, 2019.

[9] M. Altunbay, R. Martain, and M. Robinson, "Capillary pressure data from NMR logs and its implications on field economics," in *SPE Annual Technical Conference and Exhibition*, pp. 2–5, New Orleans, 2001.

[10] R. Ausbrooks, N. F. Hurley, and A. May, "Pore-size distribution in vuggy carbonates from core images, NMR and capillary pressure," in *SPE Annual Technical Conference and Exhibition*, pp. 3–5, Houston, 1999.

[11] Y. Nakashima and T. Kikuchi, "Estimation of the apertures of water-saturated fractures by nuclear magnetic resonance well logging," *Geophysical Prospecting*, vol. 55, no. 2, pp. 235–254, 2007.

[12] C. Liu, A. X. Wu, S. H. Yin, and X. Chen, "Nonlinear chaotic characteristic in leaching process and prediction of leaching cycle period," *Journal of Central South University*, vol. 23, no. 11, pp. 2935–2940, 2016.

[13] R. D. Peng, H. P. Xie, and Y. Ju, "Computation method of fractal dimension for 2-D digital image," *Journal of China University of Mining and Technology*, vol. 33, no. 1, pp. 19–24, 2004.

[14] R. D. Peng, Y. C. Yang, Y. Ju, L. T. Mao, and Y. M. Yang, "Computation of fractal dimension of rock pores based on gray CT images," *Chinese Science Bulletin*, vol. 56, no. 31, pp. 3346–3357, 2011.

[15] Y. R. Li and R. Q. Huang, "Relationship between joint roughness coefficient and fractal dimension of rock fracture surfaces," *International Journal of Rock Mechanics and Mining Sciences*, vol. 75, pp. 15–22, 2015.

[16] T. Hamm and I. Steinwart, "Adaptive learning rates for support vector machines working on data with low intrinsic dimension," *Annals of Statistics*, vol. 49, no. 6, pp. 3153–3180, 2021.

[17] K. Zhang, Y. L. Chen, W. H. Fan, X. Liu, H. Luan, and J. Xie, "Influence of intermittent artificial crack density on shear fracturing and fractal behavior of rock bridges: experimental and numerical studies," *Rock Mechanics and Rock Engineering*, vol. 53, no. 2, pp. 553–568, 2020.

[18] Y. B. Yao, J. Liu, D. M. Liu, J. Chen, and Z. Pan, "A new application of NMR in characterization of multiphase methane and adsorption capacity of shale," *International Journal of Coal Geology*, vol. 201, pp. 76–85, 2019.

[19] Y. Li, Y. H. Fu, and J. L. Chen, "Analysis on the changes of permeability of rare earth and its causes under different concentrations ore," *Mining Research and Development*, vol. 38, no. 12, pp. 117–120, 2018.

[20] R. H. Xie, L. Z. Xiao, and S. Q. Fu, "Temperature effect of nmr surface relaxation in water saturated rocks," *Journal of China University of Petroleum*, vol. 32, no. 2, pp. 45–52, 2008.

[21] W. D. Lu, L. Z. Xiao, W. Li, and D. Xiao, "Effects of diffusion due to internal gradients on NMR response in rocks," *Progress in Geophysics*, vol. 22, no. 2, pp. 556–561, 2007.

[22] M. Yang, J. C. Bi, and G. Z. Hu, "Influence of extreme temperature on the pore and fracture development of high- rank coal," *Advances in Civil Engineering*, vol. 2018, Article ID 4529751, 8 pages, 2018.

[23] W. Xu, Y. Z. Rao, D. Wang, L. Shi, and Y. Li, "Effect of pore radius distribution on infiltration of ion-absorbed rare earth ore," *Journal of Jiangxi University of Science and Technology*, vol. 41, no. 1, pp. 57–63, 2020.

[24] W. Chen and H. X. Du, "Pore analysis of high strength and high-performance concrete at high temperature based on CT test," *Concrete*, vol. 2018, no. 6, pp. 6–8, 2018.

[25] X. X. Cao, M. M. Feng, and K. H. Yuan, "Dynamic mechanical properties and damage mechanism of freeze-thaw sandstone under acid corrosion," *Geofluids*, vol. 2021, Article ID 7335284, 15 pages, 2021.

[26] Q. Y. Ma and Z. M. Cao, "Experimental study on fractal characteristics and energy dissipation of stabilized soil based on SHPB test," *Journal of Materials in Civil Engineering*, vol. 31, no. 11, pp. 1943–1959, 2019.

[27] R. Herfkens, L. Crooks, P. Davis et al., "Application of nuclear magnetic resonance (NMR) of hydrogen to the study of pathologic anatomy of the rat," *Investigative Radiology*, vol. 15, no. 5, p. 433, 1980.

[28] H. M. Zhang, G. S. Yang, and Y. Liang, "Experimental study on damage deterioration and tensile characteristics of rock under freeze-thaw environment," *Advanced Materials Research*, vol. 518-523, pp. 1749–1752, 2012.

[29] Y. F. Deng, X. B. Yue, S. Y. Liu, Y. Chen, and D. Zhang, "Hydraulic conductivity of cement-stabilized marine clay with metakaolin and its correlation with pore size distribution," *Engineering Geology*, vol. 193, pp. 146–152, 2015.

[30] X. Fukun, M. Xin, L. Lianchong et al., "Thermos-solid-gas coupling dynamic model and numerical simulation of coal containing gas," *Geofluids*, vol. 2020, Article ID 8837425, 9 pages, 2020.

[31] A. Gusso and L. Mello, "Fractal dimension of basin boundaries calculated using the basin entropy," *Chaos, Solitons & Fractals*, vol. 153, no. 2, pp. 111532–111540, 2021.

[32] Z. Minghua, Z. L. D. Jie, and Y. Pingbao, "Fractal theory-based study of the permeability of fly ash," *Journal of Hunan University (Natural Sciences)*, vol. 42, no. 1, pp. 75–80, 2015.

[33] J. Yang, J. J. Chen, Z. X. Yang, and H. L. Zheng, "A study of pore structure, pore fractal feature and permeability of unconsolidated sand," *Hydrogeology & Engineering Geology*, vol. 35, no. 3, pp. 93–98, 2008.